ACS APPLIED MATERIALS & INTERFACES

RESEARCH ARTICLE

www.acsami.org

Covalent Assembly of Gold Nanoparticles for Nonvolatile Memory Applications

Raju Kumar Gupta,[†] Damar Yoga Kusuma,[‡] P. S. Lee,[‡] and M. P. Srinivasan*[,†]

[†]Department of Chemical and Biomolecular Engineering, National University of Singapore, 4 Engineering Drive 4, Singapore, 117576

[‡]School of Materials Science and Engineering, Nanyang Technological University, 50 Nanyang Avenue, Singapore, 639798

Supporting Information

ABSTRACT: This work reports a versatile approach for enhancing the stability of nonvolatile memory devices through covalent assembly of functionalized gold nanoparticles. 11-mercapto-1-undecanol functionalized gold nanoparticles (AuNPs) with a narrow size distribution and particle size of about 5 nm were synthesized. Then, the AuNPs were immobilized on a SiO_2 substrate using a functionalized polymer as a surface modifier. Microscopic and spectroscopic techniques were used to characterize the AuNPs and their morphology before and after immobilization. Finally, a metal-insulator-semiconductor (MIS) type memory device with such covalently anchored AuNPs as a charge trapping layer was fabricated. The MIS structure showed well-defined counterclockwise $C-V$ hysteresis curves indicating a good memory effect. The flat band voltage shift was 1.64 V at a swapping voltage between ±7 V. Furthermore, the MIS structure showed a good retention characteristic up to 20 000 s. The present synthetic route to covalently immobilize gold nanoparticles system will be a step towards realization for the nanoparticle-based electronic devices and related applications.

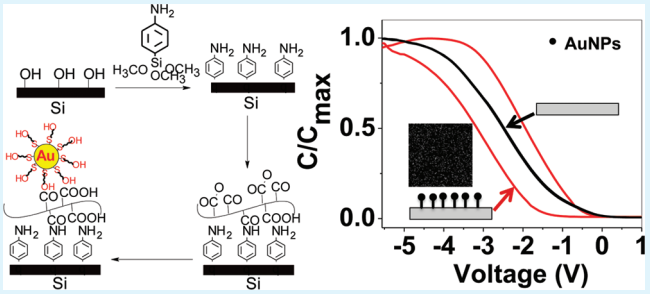

KEYWORDS: covalent assembly, gold nanoparticles, functionalization, nonvolatile memory

INTRODUCTION

Nonvolatile memory based on the floating gate structure plays an important role in portable electronic devices for its advantages of nonvolatility and low power consumption. However, floating-gate-based flash memory has been reported to have limits in continuous scaling because of increased cell-to-cell interference and nonscalable tunneling oxide thickness in terms of reliability.[1−3] To address this, discrete nanocrystals as a charge storage layer have recently been investigated to replace the electrical continuous poly-Si layer in the floating gate structure.[4−6] Flash memory devices that use discrete nanocrystals as charge-storage centers instead of a poly-Si layer could result in reduction of charge loss and therefore allow further scaling of the memory device structure.

Different kinds of nanocrystals, such as Au, Pt, Ag, W, Ni, Al, Ru, Zn, Si, Ge, $SrTiO_3$, and Al_2O_3 have been prepared and their electrons storage abilities are studied.[7−18] Silicon and germanium were initially being used as nanoparticle materials because of their compatibility with silicon technology. However, compared to their semiconductor counterparts, metallic nanoparticles are preferred because of their stronger coupling with the conduction channel, higher density of states around the Fermi level, smaller energy disturbance, and larger work function resulting in improved data retention for memory devices operating at low voltages.[19−23] Recent research articles have summarized the work on nanoparticle-based organic memories.[24−29] The main operating mechanisms discussed are an electric-field-induced charge transfer between the nanoparticles and the surrounding conjugated compounds,[30−35] filamentary conduction,[36,37] charge trapping−detrapping,[38,39] and space-charge field inhibition of injection in the nanoparticles through a high-voltage pulse.[24,40]

So far, expensive processes such as vacuum evaporation or high-temperature processing have been mainly used to form nanoparticles for the nanoparticle-based memory devices. Moreover, organic layers are susceptible to damage because of thermal budget,[41] and the resulting nanoparticles are nonuniform in size and shape during these processes. For the realization of metallic nanoparticle memory devices, requirements include the formation of high density and uniformly distributed nanoparticles.[22,42] A large spatial density enhances the charge storing capability of the floating layer, whereas a high degree of size uniformity ensures reproducible storage characteristics. Shortcomings of metallic contamination, formation of metal compounds, and nonuniformity in size and shape of metallic nanoparticles in the above mentioned memory devices can be overcome by including readymade nanoparticles in the devices.[43,44] In the case of pre-synthesized nanoparticles used in spin-coating-based

Received: August 2, 2011
Accepted: October 24, 2011
Published: October 24, 2011

Scheme 1. Immobilization of MUD-Capped Gold Nanoparticles on to a Hydroxyl-Terminated Silicon Surface

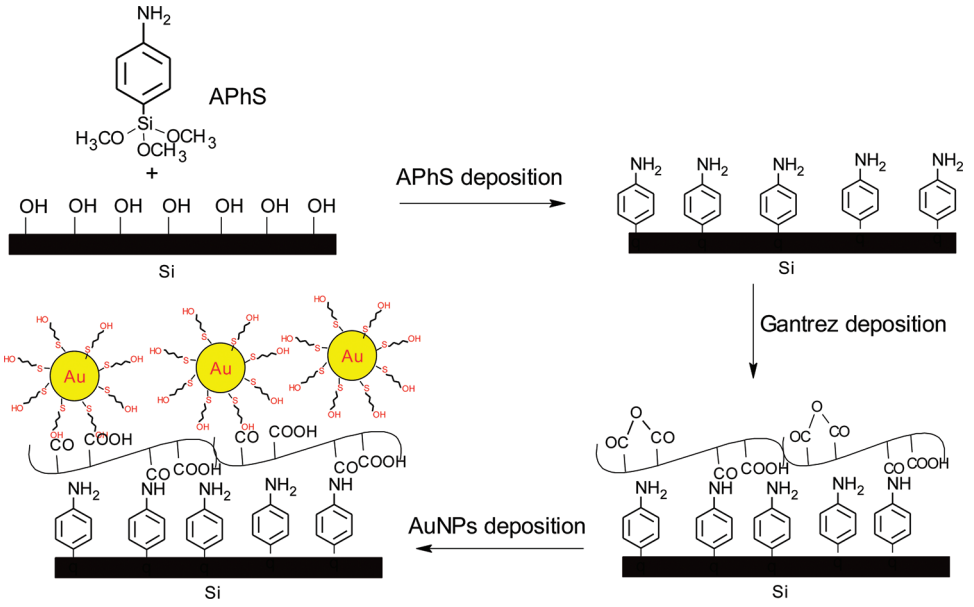

memory devices, spun cast polymer nanoparticle blends where nanotraps are randomly distributed throughout the host matrix result in uncontrolled nature of particle size distribution. Randomly distributed nanoparticles may show nonuniform device performance, because there are different numbers of nanoparticles within each unit device. Assembly of readymade nanoparticles for nonvolatile memory applications may lead a solution to above mentioned problems. The Langmuir–Blodgett deposition of organically passivated gold nanoparticles has been reported for flash memory application,[39] but these films are not mechanically robust because of weak interlayer bonding. A self-assembled monolayer of Pt nanoparticles utilizing a surface modifier was studied as a charge trapping layer for nonvolatile memory applications.[45] However, stability of assembled nanoparticles was not studied using methods such as sonication.

The use of polymeric surfaces in controlling nanoparticles at a surface is of particular interest because polymer structure and functionality can be readily manipulated via various synthetic routes. Also, polymeric surfaces provide more binding sites for further assembly as compared to monomers. Many attachment methods, including hydrogen bonding,[46−48] gold−thiol bonding,[49] and electrostatic interactions,[50−52] have been used to assemble nanoparticles at polymer surfaces. Because these methods do not produce a strong covalent linkage between the particles and the substrates, the stability of these systems over a wide range of environmental conditions (i.e., solvent, temperature, ion concentration, etc.) is restricted, which in turn limits their applicability. The stability of organic thin films has emerged as one of the critical issues in organic electronic devices since degradation of organic devices occurs largely due to changes in morphology, loss of interfacial adhesion and interdiffusion of components.[53] Covalently assembled materials could provide higher stability to the product thin film, allowing it to withstand harsh conditions such as extreme pH or extreme ionic strength. Recently, we have demonstrated that ultrathin oligoimide films formed on amine-terminated substrates via covalent assembly are better than spin-coated films in terms of stability or strength.[54,55]

In this work, we report synthesis and covalent immobilization of 11-mercapto-1-undecanol functionalized AuNPs on a SiO_2 substrate using gantrez polymer as a surface modifier. Transmission electron microscopy (TEM), X-ray photoelectron spectroscopy (XPS), field emission scanning electron microscopy (FESEM) and atomic force microscopy (AFM) were employed to investigate particle morphology, surface modification of the nanoparticles and their covalent immobilization on silicon surface. The stability of immobilized nanoparticles was tested by sonication and no noticeable change in the density of nanoparticles was observed as confirmed by FESEM. In addition, the electrical characterization of covalently bound AuNPs as a charge trapping layer in nonvolatile memory applications was also investigated. The extent of the memory window observed for such covalently anchored AuNPs was similar to the electron-beam evaporated gold nanoparticles.[56] Memory devices fabricated from covalently assembled nanoparticles has several advantages such as solution processability, enhanced device stability, low cost, and low-temperature process, which may be an attractive alternative to the expensive electron-beam evaporation technique. To the best of our knowledge, this work represents the first attempt to fabricate a MIS device using covalently attached functionalized gold nanoparticles.

EXPERIMENTAL SECTION

Procedures. *Synthesis and Immobilization of Thiol-Stabilized Gold Nanoparticles.* Details for experimental procedure can be found in the Supporting Information. Briefly, synthesis of gold nanoparticles was carried out as described in the literature.[57] Assembly of aminosilane, APhS, on Si substrate was performed as described earlier.[58] The amine-terminated substrates were immersed in a 0.5 % (w/v) THF solution of Gantrez for 1 h under nitrogen environment. The substrates were removed from the solution, rinsed vigorously, and sonicated for 5 min with THF, rinsed again with THF, finally blown dry with nitrogen. Thus obtained anhydride-terminated silicon surfaces were immersed in a 100 μg/mL solution of MUD capped nanoparticles in DMF. The contents of the flask were held at 90 °C for 1 h with stirring. Subsequently, the

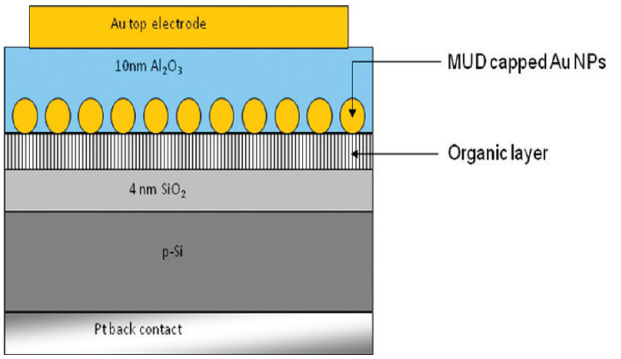

Figure 1. MIS device configuration for the immobilized MUD-capped Au nanoparticles.

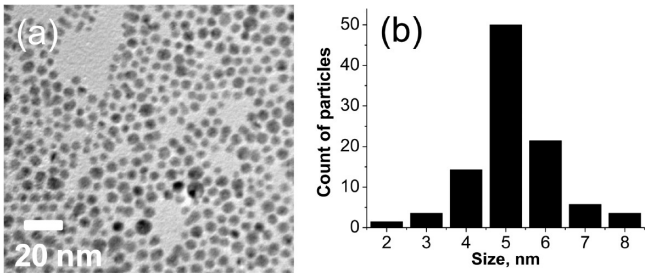

Figure 2. (a) TEM image of MUD-capped gold nanoparticles, (b) size distribution of MUD-capped gold nanoparticles.

substrates were rinsed with DMF followed by sonication for 5 min in DMF to remove any physically bound nanoparticles. Details of various deposition steps are shown in Scheme 1.

Characterization. Samples for TEM (JEM-2010 TEM (JEOL)) were prepared by placing a drop of the nanoparticle-containing solution on 3-mm formvar/carbon-coated copper grids (Electron Microscopy Sciences). Excess solution was removed by an absorbent paper and the sample was dried overnight in air before scanning. The size distribution of particles was determined by taking the sizes of 100 particles, which indicated the mean diameter and its standard deviation. XPS measurements were made on a Kratos Analytical AXIS HSi spectrometer with a monochromatized AlKα X-ray source (1486.6 eV photons) at a constant dwell time of 100 ms and a pass-energy of 40 eV. The X-ray source was run at a reduced power of 150 W. The pressure in the analysis chamber was maintained at 7.5×10^{-9} Torr or lower during each measurement. All binding energies (BEs) were referenced to the C1s hydrocarbon peak at 284.6 eV. In curve fitting, the full width at half-maximum (FWHM) for the Gaussian peaks was maintained constant for all components in a particular spectrum. The surface morphology of the films was examined by AFM (Atomic Force Microscopy NanoScope IIIa, Digital Instruments). All images were collected in air using the tapping mode and a monolithic silicon tip. The drive frequency was 330 + 50 kHz, and the voltage was between 3.0 and 4.0 V. The drive amplitude was about 300 mV and the scan rate was 1.0−1.5 Hz. The surface morphology of the nanoparticle containing films was examined by FESEM (JSM-6700F, JEOL Japan) with EDS attachment. The memory behavior of the MIS device is investigated by means of capacitance-voltage ($C-V$) and capacitance decay ($C-t$) measurements. All measurements were performed using HP4284A Precision LCR meter at frequency of 100 kHz.

MIS Capacitor Fabrication. A metal-insulator-silicon (MIS) capacitor device was fabricated. Following the incorporation of gold nanoparticle, a pulsed laser deposition (PLD) method was used to deposit 10 nm thick Al_2O_3 control oxide. Au top electrodes (0.3 mm diameter size) are then sputter-deposited using shadow mask technique subsequently. After removing the oxide, Pt film was deposited as the back side contact. The MIS device configuration is shown in Figure 1.

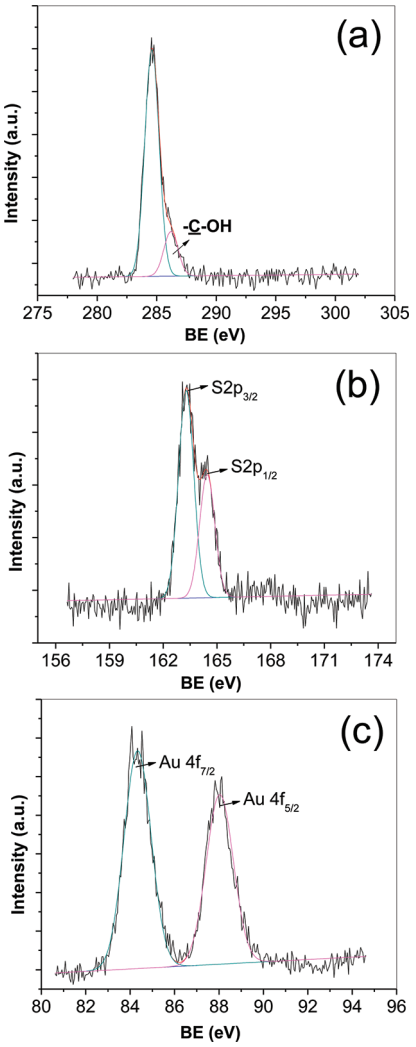

Figure 3. X-ray photoelectron spectra of MUD-capped gold nanoparticles showing the (a) C 1s region, (b) S 2p region, and (c) Au 4f region.

RESULTS AND DISCUSSION

Synthesis of MUD-Capped Gold Nanoparticles. Figure 2a shows the TEM micrograph of synthesized MUD-capped gold nanoparticles, and Figure 2b shows the size distribution for the AuNPs. The image shows that the nanoparticles are approximately spherical, with an average Au core diameter of 5 ± 0.5 nm. Figure 3 shows the XPS spectra for synthesized MUD-capped gold nanoparticles. Figure 3a shows the C1s region for the sample with the C−O component at 286.2 eV, confirming the presence of alcohol functionality. Figure 3b represents the S2p region, with peak observed at 163.3 eV and 164.4 eV corresponding to the thiolates which confirms the absence of unreacted thiol species.[59] No evidence of oxidation of the sulfur was observed for which extra sulfur peaks would occur at 168.1 eV and 169.0 eV corresponding to sulfones/sulfates. The Au $4f_{7/2}$ and Au $4f_{5/2}$ bands occur at 84.3 eV and 87.9 eV, respectively (Figure 3c). There is slight shift to higher binding energy when compared to

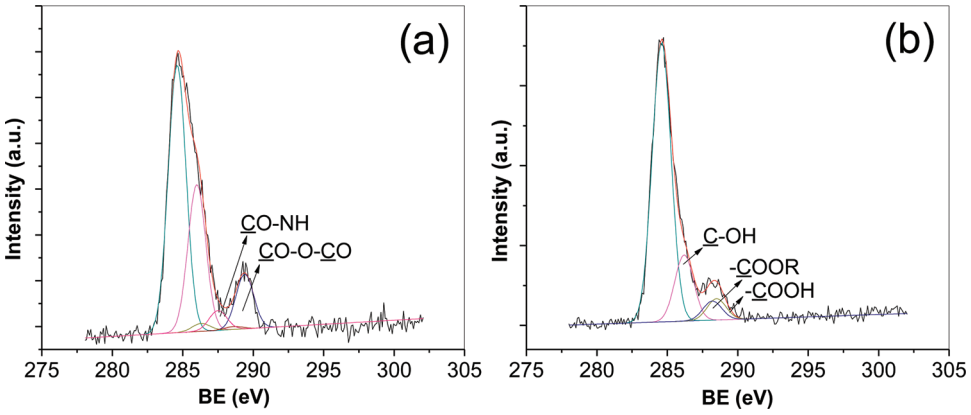

Figure 4. C1s core-level XPS spectra at various steps of the AuNPs assembly: (a) the gantrez deposited APhS substrate, (b) MUD-capped gold nanoparticles immobilized on Si substrate.

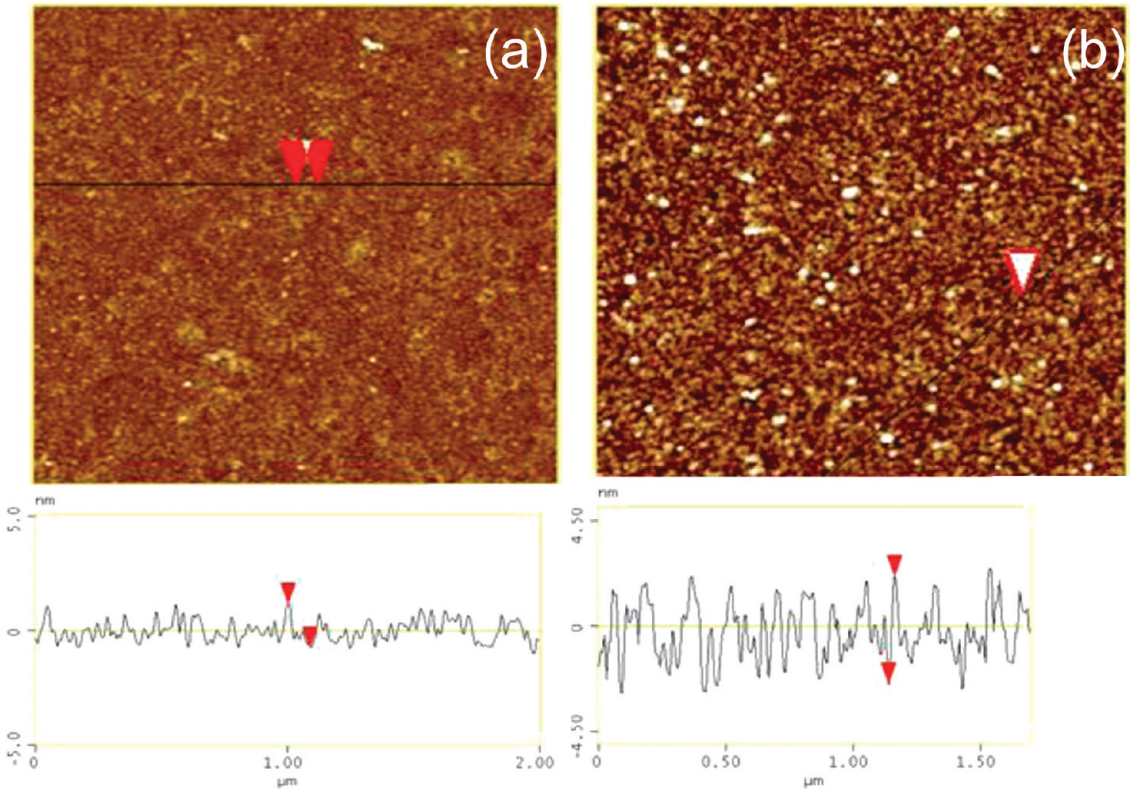

Figure 5. Tapping mode AFM images ($2 \times 2\ \mu m^2$) and z profiles for: (a) a gantrez deposited Si surface, (b) similar surface after immobilization of MUD-capped gold nanoparticles.

that for bulk nanoparticles, which is probably due to a shift in the Fermi level as the particle size is decreased. These shifts have also been reported elsewhere.[60−62]

Immobilization of MUD-Capped Gold Nanoparticles. Successful reaction between amino moieties and anhydrides of gantrez is confirmed by presence of the C1s peak components for amide formation at 287.5 eV (−CO−NH−) and presence of anhydrides at 289.4 eV (−CO−O−CO−) as shown in Figure 4a. MUD-capped AuNPs is anchored to the substrate with one of its terminal alcohol groups reacted with the anhydride on the gantrez, forming esters. C1s spectrum (Figure 4b) contains peak components for acid (−COOH) at 288.5 eV and ester (−COOR) at 288.2 eV. Also the presence of C−O component at 286.2 eV confirms the presence of alcohol functionality coming from MUD capped AuNPs. Figure 5 shows AFM images of a gantrez deposited Si substrate and immobilized AuNPs on Si substrate. The root-mean-square (RMS) roughness for the gantrez deposited image is 0.4 nm, confirming smooth surface after deposition of gantrez film; whereas that in the immobilized nanoparticle image is 1.4 nm. The image shows a single layer of nanoparticles, with some height fluctuations. The nanoparticle layer average height, measured at voids in the layer, is 4.5−5 nm, in agreement with the nanoparticle size distribution (Figure 2). This indicates that the film was composed of one layer of MUD-capped

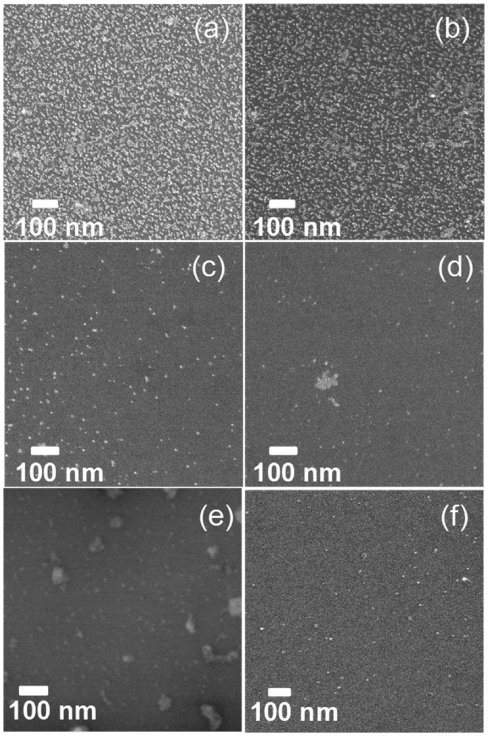

Figure 6. FESEM images for MUD-capped AuNPs immobilized on Si surface through covalent binding: (a) after rinsing, (b) after 5 min sonication; MUD-capped AuNPs solution spin-coated on gantrez deposited Si surface: (c) before sonication, (d) after 5 min sonication; MUD-capped AuNPs immobilized on APhS deposited Si surface through hydrogen binding: (e) after rinsing, (f) after 5 min sonication.

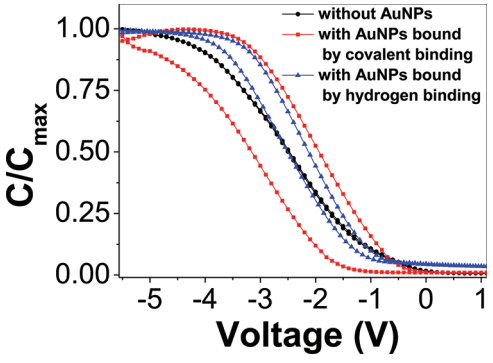

Figure 7. Normalized $C-V$ characteristics at 100 kHz obtained by biasing the top electrodes at ±6 V for control sample (without gold nanoparticle) and with gold nanoparticle.

AuNPs. The nanoparticle distribution obtained from AFM was homogeneous in different areas of the sample, confirming uniform deposition of nanoparticles over the substrate. The FESEM image (Figure 6a) shows the presence of the gold nanoparticles as highly dispersed and well separated, showing no evidence of aggregation during the immobilization step. The films were imaged as is and not sputtered-coated with a conductive layer of platinum, because they contain sufficient gold present to avoid charging the samples by the electron beam. Stability of these anchored nanoparticles was checked by performing sonication of the substrate-bound nanoparticle systems in DMF for 5 min. Figure 6b shows FESEM image after the sonication step.

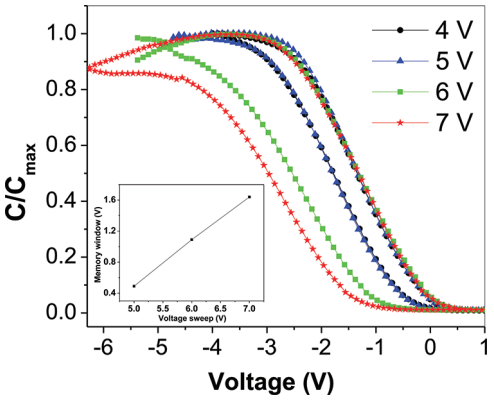

Figure 8. $C-V$ characteristics at 100 kHz under different scan voltage ranges for an MIS capacitor incorporating covalently immobilized gold nanoparticles. The inset shows the hysteresis as a function of the bias voltage limits.

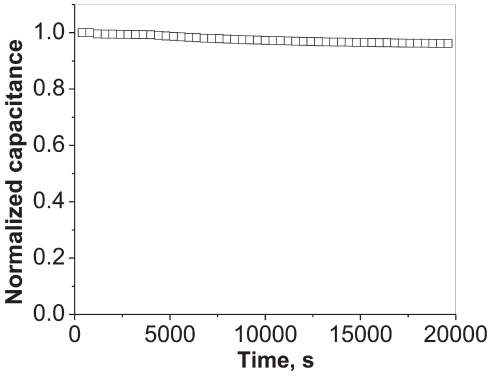

Figure 9. Charge retention characteristics (normalized capacitance) of the MIS device at 100 kHz after programming at +5 V.

There is no loss of particles because of sonication, thereby ensuring that the particles were indeed firmly attached to the substrates. The nanoparticle density after the sonication step is calculated to be 5×10^{11} cm^{-2}. To further explore the need of anchoring the nanoparticles, we spin-coated the same nanoparticle solution on a gantrez-modified surface. OH-terminated MUD-capped AuNPs were also deposited on an amine-terminated APhS surface and immobilized through hydrogen binding. In both the cases, density of the nanoparticles is less when compared to that obtained from the covalent immobilization step (Figure 6c,e). Also, distribution of the nanoparticles is not uniform over the surface and aggregation of the particles was observed, possibly due to hydrogen bonding between them. Stability of the immobilized nanoparticles was investigated by sonicating the particle-laden substrate. Figure 6d,f show loss of nanoparticles from the surface subsequent to sonication. The stability of citrate-stabilized AuNPs immobilized on APhS surface was tested by immersing the substrate in pH 10-buffered solution. The number density of AuNPs immobilized on APhS surface (see Figure S1a in the Supporting Information) decreased after immersion in buffered solution (see Figure S1b in the Supporting Information). This loss of nanoparticles might be due to deprotonation of amines on APhS at pH 10, resulting in the loss of electrostatic binding between the AuNPs and amines. This clearly demonstrates the need of covalent binding of

nanoparticles to obtain stable device structures for nanoparticle-based electronic devices.

***C*−*V* and *C*−*t* Analysis.** Normalized *C*−*V* hysteresis curves of the MIS memory device containing the covalently bound AuNPs are shown in Figure 7. Counter-clockwise *C*−*V* hysteresis curves with large width were obtained. The observed counter-clockwise hysteresis for the MIS device with nanoparticles indicates net positive charging, which should be due to hole trapping from the substrate accumulation layer into the nanoparticles.[38] The device without AuNPs shows a negligible memory window at 6/−6 V for its program/erase voltage. In contrast, clear hysteresis window of 1.1 V was observed for the sample with gold nanoparticles immobilized through covalent binding. Both MIS devices are fabricated using the same procedure, except for the addition of the gold nanoparticles. The observed hysteresis effect, therefore, could be related to the charging of the nanoparticles and nanoparticle-related traps. Further, a hysteresis window of only 0.34 V was observed for the sample having AuNPs immobilized on APhS-modified Si surface through hydrogen binding; this may be due to lower nanoparticle number density as compared to that observed for covalently immobilized AuNPs. Hence, the density of gold nanoparticles is a critical parameter for the hysteresis window. As shown in Figure 8, the hysteresis window of the *C*−*V* curve for sample having covalently immobilized AuNPs increases from 0.49 to 1.64 V with increasing maximum operating bias from 5 to 7 V, indicating that more holes are being trapped in the nanoparticles as the sweeping bias is increased.[63] There is little or negligible shift in the initial flatband voltage upon increasing the operation bias, indicating minimal influence of interface traps. The extent of the observed memory window is similar to the previously reported value (1.5 V at ±7 V) for electron-beam evaporated gold nanoparticles.[56] Thus, memory devices fabricated from solution processable covalently assembled nanoparticles may be an alternative to expensive electron-beam evaporation technique due to their low cost and ease of fabrication. Capacitance decay (C-t) measurement was conducted to evaluate the charge retention properties of the device. A charging bias of +5 V was applied to the device for 1 min to facilitate charge injection into the nanoparticles. Subsequently, the capacitance was monitored as a function of time under the flat-band condition of the device. The immobilized AuNPs device shows good retention characteristics up to 20 000 s (Figure 9). The observed behavior indicates good suppression of charge losses via vertical and lateral charge diffusion,[64] which could be an early indicator for a good, well-dispersed nanoparticle distribution.

CONCLUSIONS

In summary, we have successfully described the surface functionalization capability of gold nanoparticles prepared with 11-mercapto-1-undecanol, a bifunctional ligand acting as a surfactant. Detailed structural characterizations have been performed for covalently immobilized gold nanoparticles on silicon surface. XPS confirmed covalent attachment of functionalized gold nanoparticles on to the silicon substrate. FESEM and AFM images show the surface morphology of the immobilized nanoparticles. Immobilized nanoparticles are well-separated and stable against sonication as compared to spin coated nanoparticles. Covalent bound gold nanoparticles showed stable charge storage capacity along with advantages of ease of processing and low cost as compared to expensive electron-beam evaporation set up.

ASSOCIATED CONTENT

Supporting Information. Experimental section and FESEM images for citrate-stabilized AuNPs immobilized on APhS surface. This material is available free of charge via the Internet at http://pubs.acs.org.

AUTHOR INFORMATION

Corresponding Author

*Tel: +65-65162171. Fax: +65-67791936. E-mail: chesmp@nus.edu.sg.

ACKNOWLEDGMENT

The authors thank the National University of Singapore for providing financial support for this project and a scholarship for R.K.G.

REFERENCES

(1) Tiwari, S.; Rana, F.; Chan, K.; Hanafi, H.; Chan, W.; Buchanan, D. *Tech. Dig.—Int. Electron Devices Meet.* **1995**, *1995*, 521.

(2) Kim, K.; Lee, S. Y. *Microelectron. Eng.* **2007**, *84* (9-10), 1976–1981.

(3) Bez, R.; Camerlenghi, E.; Modelli, A.; Visconti, A. *Proc. IEEE* **2003**, *91* (4), 489–501.

(4) Tiwari, S.; Rana, F.; Hanafi, H.; Hartstein, A.; Crabbé, E. F.; Chan, K. *Appl. Phys. Lett.* **1996**, *68* (10), 1377–1379.

(5) Tu, C. H.; Chang, T. C.; Liu, P. T.; Liu, H. C.; Sze, S. M.; Chang, C. Y. *Appl. Phys. Lett.* **2006**, *89* (16), 162105.

(6) De Blauwe, J. *IEEE Trans. Nanotechnol.* **2002**, *1* (1), 72–77.

(7) Chen, J. H.; Yoo, W. J.; Chan, D. S. H.; Tang, L. J. *Appl. Phys. Lett.* **2005**, *86* (7), 1–3.

(8) Kim, J. H.; Baek, K. H.; Kim, C. K.; Kim, Y. B.; Yoon, C. S. *Appl. Phys. Lett.* **2007**, *90* (12), 123118.

(9) Lee, J. J.; Harada, Y.; Pyun, J. W.; Kwong, D. L. *Appl. Phys. Lett.* **2005**, *86* (10), 1–3.

(10) Normand, P.; Kapetanakis, E.; Tsoukalas, D.; Kamoulakos, G.; Beltsios, K.; Van Den Berg, J.; Zhang, S. *Mater. Sci. Eng., C* **2001**, *15* (1-2), 145–147.

(11) Park, B.; Cho, K.; Moon, B. M.; Kim, S. *Microelectron. Eng.* **2007**, *84* (5-8), 1627–1630.

(12) Samanta, S. K.; Yoo, W. J.; Samudra, G.; Tok, E. S.; Bera, L. K.; Balasubramanian, N. *Appl. Phys. Lett.* **2005**, *87* (11), 1–3.

(13) Wang, Y. Q.; Chen, J. H.; Yoo, W. J.; Yeo, Y. C.; Kim, S. J.; Gupta, R.; Tan, Z. Y. L.; Kwong, D. L.; Du, A. Y.; Balasubramanian, N. *Appl. Phys. Lett.* **2004**, *84* (26), 5407–5409.

(14) Yang, F. M.; Chang, T. C.; Liu, P. T.; Chen, U. S.; Yeh, P. H.; Yu, Y. C.; Lin, J. Y.; Sze, S. M.; Lou, J. C. *Appl. Phys. Lett.* **2007**, *90* (22), 222104.

(15) Yim, S. S.; Lee, M. S.; Kim, K. S.; Kim, K. B. *Appl. Phys. Lett.* **2006**, *89* (9), 093115.

(16) Yuan, C. L.; Darmawan, P.; Setiawan, Y.; Lee, P. S.; Ma, J. *Appl. Phys. Lett.* **2006**, *89* (4), 043104.

(17) Chan, K. C.; Lee, P. F.; Dai, J. Y. *Appl. Phys. Lett.* **2008**, *92* (22), 223105.

(18) Lee, P. F.; Lu, X. B.; Dai, J. Y.; Chan, H. L. W.; Jelenkovic, E.; Tong, K. Y. *Nanotechnology* **2006**, *17* (5), 1202–1206.

(19) Dufourcq, J.; Bodnar, S.; Gay, G.; Lafond, D.; Mur, P.; Molas, G.; Nieto, J. P.; Vandroux, L.; Jodin, L.; Gustavo, F.; Baron, T. *Appl. Phys. Lett.* **2008**, *92* (7), 073102.

(20) Hou, T. H.; Ganguly, U.; Kan, E. C. *IEEE Electron Device Lett.* **2007**, *28* (2), 103–106.

(21) Lee, C.; Meteer, J.; Narayanan, V.; Kan, E. C. *J. Electron. Mater.* **2005**, *34* (1), 1–11.

(22) Liu, Z.; Lee, C.; Narayanan, V.; Pei, G.; Kan, E. C. *IEEE Trans. Electron Devices* **2002**, *49* (9), 1606–1613.

(23) Sargentis, C.; Giannakopoulos, K.; Travlos, A.; Tsamakis, D. *Surf. Sci.* **2007**, *601* (13), 2859–2863.
(24) Bozano, L. D.; Kean, B. W.; Beinhoff, M.; Carter, K. R.; Rice, P. M.; Scott, J. C. *Adv. Funct. Mater.* **2005**, *15* (12), 1933–1939.
(25) Ling, Q. D.; Liaw, D. J.; Zhu, C.; Chan, D. S. H.; Kang, E. T.; Neoh, K. G. *Prog. Polym. Sci.* **2008**, *33* (10), 917–978.
(26) Scott, J. C.; Bozano, L. D. *Adv. Mater.* **2007**, *19* (11), 1452–1463.
(27) Yang, Y.; Ouyang, J.; Ma, L.; Tseng, R. J. H.; Chu, C. W. *Adv. Funct. Mater.* **2006**, *16* (8), 1001–1014.
(28) Prime, D.; Paul, S. *Philos. Trans. R. Soc. London, Ser. A* **2009**, *367* (1905), 4141–4157.
(29) Tsoukalas, D. *Philos. Trans. R. Soc. London, Ser. A* **2009**, *367* (1905), 4169–4179.
(30) Lai, P. Y.; Chen, J. S. *Appl. Phys. Lett.* **2008**, *93* (15), 153305.
(31) Ouyang, J.; Chu, C. W.; Sieves, D.; Yang, Y. *Appl. Phys. Lett.* **2005**, *86* (12), 1–3.
(32) Prakash, A.; Ouyang, J.; Lin, J. L.; Yang, Y. *J. Appl. Phys.* **2006**, *100* (5), 054309.
(33) Song, Y.; Ling, Q. D.; Lim, S. L.; Teo, E. Y. H.; Tan, Y. P.; Li, L.; Kang, E. T.; Chan, D. S. H.; Zhu, C. *IEEE Electron Device Lett.* **2007**, *28* (2), 107–110.
(34) Lin, H. T.; Pei, Z.; Chen, J. R.; Hwang, G. W.; Fan, J. F.; Chan, Y. J. *IEEE Electron Device Lett.* **2007**, *28* (11), 951–953.
(35) Ouyang, J.; Chu, C. W.; Szmanda, C. R.; Ma, L.; Yang, Y. *Nat. Mater.* **2004**, *3* (12), 918–922.
(36) Cölle, M.; Büchel, M.; de Leeuw, D. M. *Org. Electron.* **2006**, *7* (5), 305–312.
(37) Tang, W.; Shi, H.; Xu, G.; Ong, B. S.; Popovic, Z. D.; Deng, J.; Zhao, J.; Rao, G. *Adv. Mater.* **2005**, *17* (19), 2307–2311.
(38) Leong, W. L.; Lee, P. S.; Mhaisalkar, S. G.; Chen, T. P.; Dodabalapur, A. *Appl. Phys. Lett.* **2007**, *90* (4), 042906–3.
(39) Paul, S.; Pearson, C.; Molloy, A.; Cousins, M. A.; Green, M.; Kolliopoulou, S.; Dimitrakis, P.; Normand, P.; Tsoukalas, D.; Petty, M. C. *Nano Lett.* **2003**, *3* (4), 533–536.
(40) Simmons, J. G.; Verderber, R. R. *Proc. R. Soc. London, Ser. A* **1967**, *301* (1464), 77–102.
(41) Kolosov, D.; English, D. S.; Bulovic, V.; Barbara, P. F.; Forrest, S. R.; Thompson, M. E. *J. Appl. Phys.* **2001**, *90* (7), 3242–3247.
(42) Tsoukalas, D.; Dimitrakis, P.; Kolliopoulou, S.; Normand, P. *Mater. Sci. Eng., B* **2005**, *124-125* (SUPPL), 93–101.
(43) Tseng, J. Y.; Cheng, C. W.; Wang, S. Y.; Wu, T. B.; Hsieh, K. Y.; Liu, R. *Appl. Phys. Lett.* **2004**, *85* (13), 2595–2597.
(44) Kato, H.; Shibata, Y.; Kuwano, H. *Electron. Commun. Jpn., Part II: Electronics* **1987**, *70* (4), 65–73.
(45) Choi, H.; Choi, B. S.; Kim, T. W.; Jung, S. J.; Chang, M.; Lee, T.; Hwang, H. *Nanotechnology* **2008**, *19* (30), 305704.
(46) Binder, W. H.; Kluger, C.; Josipovic, M.; Straif, C. J.; Friedbacher, G. *Macromolecules* **2006**, *39* (23), 8092–8101.
(47) Binder, W. H.; Kluger, C.; Straif, C. J.; Friedbacher, G. *Macromolecules* **2005**, *38* (23), 9405–9410.
(48) Haryono, A.; Binder, W. H. *Small* **2006**, *2* (5), 600–611.
(49) Li, B.; Li, C. Y. *J. Am. Chem. Soc.* **2007**, *129* (1), 12–13.
(50) Bhat, R. R.; Genzer, J.; Chaney, B. N.; Sugg, H. W.; Liebmann-Vinson, A. *Nanotechnology* **2003**, *14* (10), 1145–1152.
(51) Russell, L. E.; Galyean, A. A.; Norte, S. M.; Leopold, M. C. *Langmuir* **2007**, *23* (14), 7466–7471.
(52) Schmitt, J.; Decker, G.; Dressick, W. J.; Brandow, S. L.; Geer, R. E.; Shashidhar, R.; Calvert, J. M. *Adv. Mater.* **1997**, *9* (1), 61–65.
(53) Liang, Z.; Dzienis, K. L.; Xu, J.; Wang, Q. *Adv. Funct. Mater.* **2006**, *16* (4), 542–548.
(54) Zhang, F.; Jia, Z.; Srinivasan, M. P. *Langmuir* **2005**, *21* (8), 3389–3395.
(55) Zhang, F.; Srinivasan, M. P. *Colloids Surf. A* **2005**, *257-258*, 295–299.
(56) Sargentis, C.; Giannakopoulos, K.; Travlos, A.; Normand, P.; Tsamakis, D. *Superlattices Microstruct.* **2008**, *44* (4-5), 483–488.
(57) Wanunu, M.; Popovitz-Biro, R.; Cohen, H.; Vaskevich, A.; Rubinstein, I. *J. Am. Chem. Soc.* **2005**, *127* (25), 9207–9215.
(58) Zhang, F.; Srinivasan, M. P. *Langmuir* **2004**, *20* (6), 2309–2314.
(59) Castner, D. G.; Hinds, K.; Grainger, D. W. *Langmuir* **1996**, *12* (21), 5083–5086.
(60) Evans, S. *Handbook of X-ray and Ultraviolet Photoelectron Spectroscopy*; Heyden & Son: London, 1977.
(61) Johnson, S. R.; Evans, S. D.; Brydson, R. *Langmuir* **1998**, *14* (23), 6639–6647.
(62) Nakamoto, M.; Yamamoto, M.; Fukusumi, M. *Chem. Commun.* **2002**, *15*, 1622–1623.
(63) Nicolean, E. H.; Brews, J. R. *Metal Oxide Semiconductor Physics and Technology*, 1st ed.; Wiley: New York, 1992.
(64) Kim, J. K.; Cheong, H. J.; Kim, Y.; Yi, J. Y.; Bark, H. J.; Bang, S. H.; Cho, J. H. *Appl. Phys. Lett.* **2003**, *82* (15), 2527–2529.